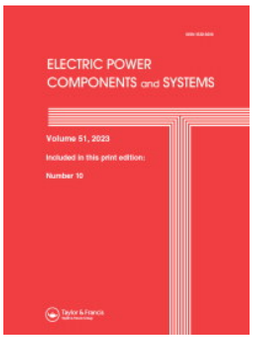

Taylor & Francis
Taylor & Francis Group

Electric Power Components and Systems

ISSN: (Print) (Online) Journal homepage: https://www.tandfonline.com/loi/uemp20

A Study on Torque Ripple Improvement Compared to a Modified Rotor and Stator Poles SRMs with Classical SRMs Using Dynamic and FFT Analysis

Hüseyin Çalik, Yusuf Özoğlu, S. Hakan Undil & Ümit Kemallettin Terzi

To cite this article: Hüseyin Çalik, Yusuf Özoğlu, S. Hakan Undil & Ümit Kemallettin Terzi (2023): A Study on Torque Ripple Improvement Compared to a Modified Rotor and Stator Poles SRMs with Classical SRMs Using Dynamic and FFT Analysis, Electric Power Components and Systems, DOI: 10.1080/15325008.2023.2196675

To link to this article: https://doi.org/10.1080/15325008.2023.2196675

Electric Power Components and Systems, 0(0): 1–10, 2023

ISSN: 1532-5008 print / 1532-5016 online
DOI: 10.1080/15325008.2023.2196675

A Study on Torque Ripple Improvement Compared to a Modified Rotor and Stator Poles SRMs with Classical SRMs Using Dynamic and FFT Analysis

Hüseyin Çalik,[1] Yusuf Özoğlu,[2] S. Hakan Undil,[3] and Ümit Kemallettin Terzi[4]

[1]Faculty of Engineering, Department of Electrical-Electronics Engineering, Istanbul University-Cerrahpaşa, Istanbul, Turkey

[2]Technical Sciences Vocational College, Control Technology Department, Istanbul University-Cerrahpaşa, Istanbul, Turkey

[3]Faculty of Engineering and Architecture, Department of Electrical Electronics Engineering, Nişantası University, Istanbul, Turkey

[4]Faculty of Technology, Department of Electrical-Electronics Engineering, University of Marmara, Istanbul, Turkey

CONTENTS

Abstract—SRMs have high torque ripples. Modifying the stator and rotor shape of SRMs is one of their methods to remove torque ripples. In this study, new rotor and stator geometries have been proposed for SRM. Performance characteristics are obtained and dynamic analyses are carried out for both novel and classical 6/4 SRMs. FFT analyses of the torque characteristics are also performed for the both SRMs. The changes in performance and the FFT results of torque characteristics are determined for both the current-controlled and uncontrolled operations in both SRMs. 23.60% and 15.20% improvements in torque ripples are achieved for the uncontrolled and current-controlled operations in SRMs respectively. When the FFT analyses are applied to the torque characteristics, the THD values are obtained as 21.19% and 8.31% in the uncontrolled and controlled motor current operations respectively. A 122 W three-phase 6/4 SRM simulation based on the MATLAB–SIMULINK environment is performed to validate the improvement of the torque ripple of the proposed model.

Keywords: switched reluctance motor, torque ripple reduction, FFT analysis

Received 26 October 2020; accepted 21 March 2023

Address correspondence to Hüseyin Çalik, Department of Electrical-Electronics Engineering, Giresun University, Giresun/Turkey E-mail: hcalik@istanbul.edu.tr

1. INTRODUCTION

Switched reluctance motor (SRM) is commonly used in industry, primarily in variable speed applications. It has a high torque/mass ratio, but a high torque ripple. Various studies are available in the literature to reduce the torque ripple; some of them suggest changes in the driver circuits [1–4], some others in the magnetic design of the motor [5–9], torque distribution, and sharing function (TSF) method function [10–13] and adaptive intelligent methods [14–21].

The new types of SRM with modified shape poles have been suggested as a result of static field analyses employing the finite elements method (FEM) [7,8]. It is realized that these new types covering only the modified design are to be improved further to incorporate the required changes

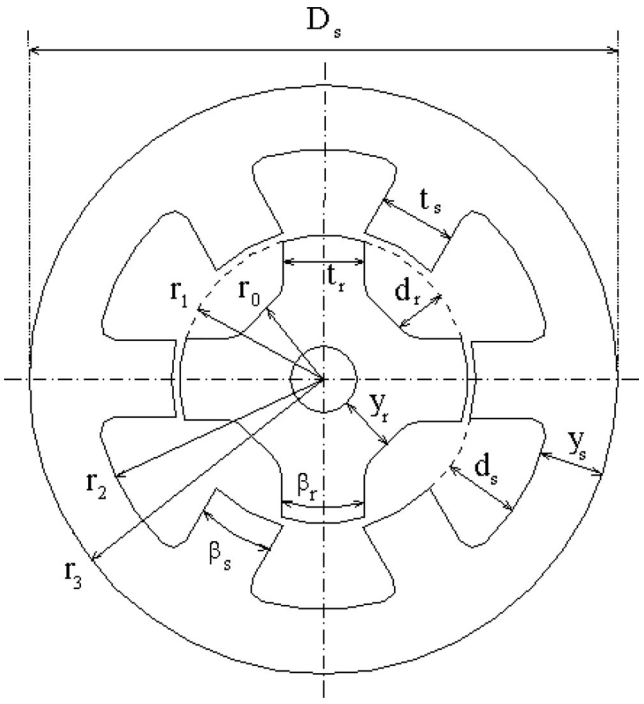

FIGURE 1. Stator and rotor dimensions of 6/4 classical SRM.

in the driver circuits of SRM and the control methods to be applied. This study aims to fill this gap.

In this study, several dynamic models including driver circuits are developed and the performance values of both classical and a new design of SRM obtained from their dynamic analyses are compared with each other, and also with the values previously obtained from the static analyses of both designs. It is concluded that the results of dynamic analyses which take both the magnetic design and the driver circuits into consideration support the results of static analyses which consider the magnetic design only, as much as the improvement in torque ripple is concerned.

2. DESIGN AND PARAMETER OF THE SRM

SRM used in this study has 3-phase and 6/4 pole construction. Geometric parameters for a 6/4 SRM with classical pole shapes are given in Figure 1 and their values are given in Table 1.

In a previous study, a novel SRM that has different pole shape geometry in both stator and rotor from that of a classical type is developed [5]. The parameters in this work are provided from the mentioned study for which the finite elements method (FEM) is applied for the static analysis to minimize the torque ripple. The SRM with classical pole shape will be referred to as SRM-I and the SRM with the

Parameter	Value	Parameter	Value
r_0	1.734·cm	d_r	0.6147·cm
r_1	2.349·cm	y_s	0.8179·cm
r_2	3.881·cm	y_r	0.8636·cm
r_3	4.699·cm	G	0.2286·cm
Ts	1.226·cm	βs	30°
Tr	1.295·cm	β_r	32°
Ds	1.508·cm		

TABLE 1. Parameters and values of the classical SRM.

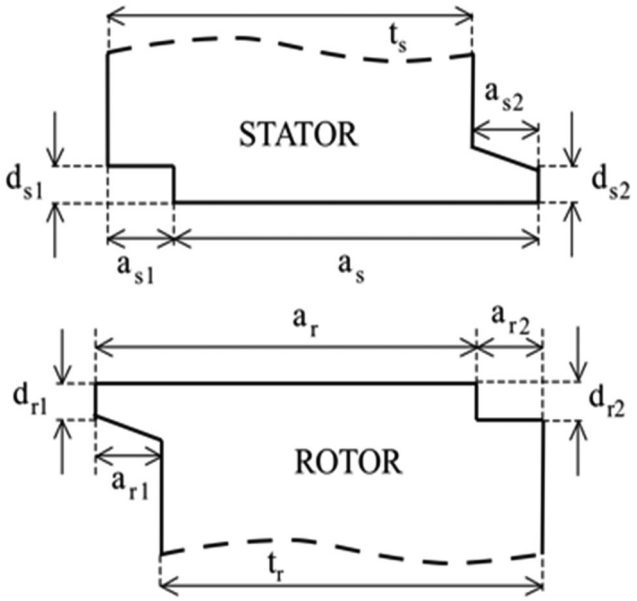

FIGURE 2. Stator and rotor pole shape of 6/4 modified SRM-II [5].

modified shaped poles as SRM-II. The pole parameters of the SRM-II are given in Figure 2, and the pole head parameter values of SRM-II are given in Table 2 [5]. In this study, it will not be discussed on which approaches the improvement in the torque is based on with the proposed model. Apart from this, it has been shown that the ripple is reduced by the results of the torque FFT analysis of the SRM-II by examining the mentioned motors under dynamic operating conditions.

3. DYNAMIC MODEL OF SRM

The dynamic characteristics of SRM consist of its electromagnetic, torque, and mechanical equations [1]. If the mutual effect of the phases is neglected, the voltage applied to one phase of SRM can be expressed as follows.

$$v_j = R_j \cdot i_j + \frac{d\lambda_j(\theta, i)}{dt} j = 1...m \tag{1.1}$$

Parameter	Value	Parameter	Value
d_{s1}	%6d_s	a_s	31°
d_{r1}	%15d_r	a_r	33°
d_{s2}	2g	a_{s1}	5°
d_{r2}	2g	a_{r2}	5°
		a_{s2}	4°
		a_{r2}	4°

TABLE 2. Pole head parameter values of SRM-II [5].

where v_j indicates the voltage applied on the phase windings, i_j represents the phase current, R_j shows the phase resistance and λ_j is the phase current and m is the motor phase number. In the SRM, flux is a function of both the current and the rotor position. Accordingly, Eq. (1.1) can be reorganized as:

$$v_j = R_j.i_j + \frac{\partial\lambda_j(\theta,i)}{\partial i_j}\cdot\frac{di_j(\theta,i)}{dt} + \frac{\partial\lambda_j(\theta,i)}{\partial\theta_j}\cdot\frac{d\theta_j}{dt} \tag{1.2}$$

where θ_j is the rotor position. When Eq. (1.2) is rearranged, the phase current can be expressed as follows:

$$\frac{di_j(\theta,i)}{dt} = \left(\frac{\partial\lambda_j(\theta,i)}{\partial i_j}\right)^{-1} \cdot\left(v_j - R_j\cdot i_j\frac{di_j(\theta,i)}{dt} + \frac{\partial\lambda_j(\theta,i)}{\partial\theta_j}\cdot\frac{d\theta_j}{dt}\right) \tag{1. 3}$$

$$i_j = \frac{\lambda_n(\theta,i)}{L_n(\theta,i)} \tag{1.4}$$

If each phase of the SRM is excited, it produces an instantaneous torque. When the instantaneous torques produced by the phases are added, the total torque induced in the motor is obtained. The instantaneous torque produced by one phase of the motor is as follows:

$$T_{ej} = \left(\frac{\partial W_j(\theta_j,i_j)}{\partial\theta_j}\right)\ i_j = \text{ constant} \tag{1.5}$$

where W_j is the co-energy.

The instantaneous torque of one phase can be rewritten as below.

$$T_{ej} = \int_0^{i_j}\frac{\partial\lambda_j(\theta_j,i_j)}{\partial\theta_j}\cdot di_j \tag{1.6}$$

The total torque of the motor can be found by adding the instantaneous torques of the phases. The total torque T_e of the motor can be written as:

$$T_e = \frac{1}{2}\frac{dL(\theta_j)}{d\theta}\cdot {i_j}^2 T_e = \sum\nolimits_{j=1} T_j(\theta_j,i_j) \tag{1.7}$$

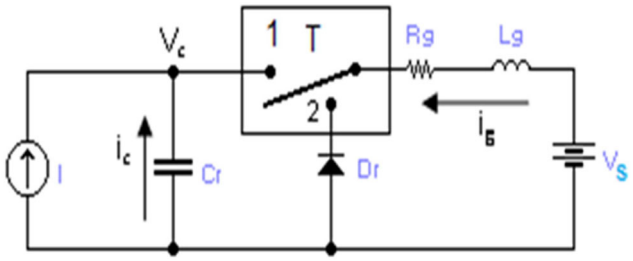

FIGURE 3. C-dump driver circuit [13].

Mechanical equations can be expressed as below:

$$T_e = J\cdot\frac{d\omega_r}{dt} + B\cdot\omega_r + T_l \tag{1.8}$$

here T_l is the load torque, ω_r is the rotor speed, J and B are the moment of inertia and the coefficient of friction respectively. When Eq. (1.8) is rearranged to write the speed expression will be achieved.

$$\frac{d\omega_r}{dt} = \frac{1}{J}(T_e - T_l + B\cdot\omega_r) \tag{1.9}$$

Position of motor shaft:

$$\theta = \int\int\frac{d\omega_r}{dt} \tag{1.10}$$

The current is obtained from Eq. (1.4) and the position of the motor shaft is obtained from Eq. (1.10). The dynamic motor model has been obtained by using Moment values obtained by FEM analysis based on position and current values. For the dynamic model of the SRM, it is also necessary to design the driver circuit. For this purpose, a C-dump driver circuit is used [22]. In the related study, a detailed analysis of the C-dump circuit is given.

3.1. Driver Circuit of SRM

A C-dump driver circuit is used to drive SRM. The simplified equivalent circuit of the single-phase C-dump driver is given in Figure 3, where I is the total current; L_g and R_g are the inductance and internal resistance of the inductor respectively. I_g is the winding current in the C-dump circuit. Vc denotes the voltage across the C-dump capacitor, C_r dumping capacitor. Vs represents supply voltage; T represents feedback switch and Dr represents feedback diode. The voltage of the C_r capacitor is usually kept at $2Vs$. The period of the switch is T. D defines the position of the T switch. $U_g = 1$ represents position 1 and U_g=0 position 2. Parameters used in the dynamic model and the driver circuit of SRM are given in Table 3 together with their

Symbol	Value	Unit
J	0.000189	kg m^2
B	0.0001	Nm s/R
K	0.005	Nm s/R
R	0.111	Ω
V_s	24	V
R_r	2.67	Ω
L_r	19.3	mH
C_r	370	uF
f_s	10^4	Hz
D	0.5	–
t_d	2.5°	degree
t_{on}	32.5°	degree

TABLE 3. SRM's and C-dump driver dynamic parameter.

values. Where j is the inertial torque; B is the viscous friction coefficient; K is the load torque coefficient; R is the phase resistance:

fs is the switching frequency and D is duty cycle of the electronic switch discharging C-dump capacitor respectively; t_d and t_{on} represent the delay and the turn-on angle, respectively.

The state equations are written as follows:

$$\frac{dv_c}{dt} = \frac{(I - u_g \cdot i_g)}{C_r} \tag{2.1}$$

$$\frac{di_g}{dt} = \frac{(u_g \cdot V_c - V_k - R_g \cdot i_g)}{L_g} \tag{2.2}$$

nth phase voltage is defined as;

$$V_n = V_k - V_k(1 - D) - (V_k - V_c) \cdot (1 - D) \cdot (1 - Z_n) \tag{2.3}$$

Where

$$Z_n = 0.5 \cdot (1 + sign(i_n)) \tag{2.4}$$

Zn defines the effect of freewheel diodes in the C-dump circuit. While nth phase current is in >1, Zn = 1 and Zn = 0 for all others.

3.2. *The MATLAB–SIMULINK Model of SRM*

Inductance, flux, and torque data obtained from static field analyses by FEM are generally used either in the form of equations (curve fitting method) or look-up tables. To generate dynamic models of the SRM-I and SRM-II, the latter method has been preferred in this study. The dynamic model of SRM obtained from MATLAB–SIMULINK is given in Figure 4. It consists of a power supply, C-dump driver, sensor, mechanical equivalent, current and speed control circuits. The dynamic analyses are carried out both in the uncontrolled mode (UnCM) and the current-controlled mode (CCM). Additionally, the torque ripple FFT analyses of the motors are performed.

Figure 4 shows the MATLAB–SIMULINK SRM model. The modeling has been obtained in such a way that a comparison of the dynamic behaviors of the two different types (SRM-I and SRM-II) is done simultaneously. The voltage is applied to both motor types, with a delay angle $td = 2.5°$, and turn-on angle ton = 32.5°.

The dynamic model of the SRM, whose block diagram is given in Figure 5, is obtained based on Eqs. (1.1) and (1.4) and the inductance profile obtained from FEM.

$T_e(\theta, i)$ produced by a phase of SRM taking phase current and rotor angle into account is taken from a look-up table. The total electromagnetic torque of the three phases is obtained using Eq. (1.7). The torque circuit of SRM is given in Figure 6.

4. RESULTS OF DYNAMIC ANALYSIS OF SRM

Dynamic analyses are realized for both the SRM-I and SRM-II types under the uncontrolled (UnCM) and the current-controlled mode with 9 A (CCM) operation modes. These modes are examined both in time and frequency domains using FFT analysis.

4.1. Dynamic Analysis in Time Domain Schemes for UnCM

Dynamic analyses of the SRM-I (classical shape pole) and the SRM-II (modified-shaped pole) have been provided under the same conditions. As mentioned before, classical and modified pole shape SRMs are referred to as SRM-I and SRM-II, therefore 1 and 2 subscripts also represent the parameters used for the SRM-I and SRM-II respectively. Both current and inductance waveforms for one phase of the SRM-I and SRM-II are given together in Figure 7 which shows that the inductance of L_2 starts rising before that of L_1.

To maintain a high torque from the motor, the phase is turned on at the lowest value of inductance so that as much current as possible flows in the winding during the rising portion of the inductance waveform. When the voltage is applied to SRM-I, the phase current rises sharply and reaches its highest value at 14.5 A. It reduces to 8 A at the end of the dwell angle and then to zero. Crossover current value during phase commutation is read as 8 A. On the other hand, when the voltage is applied to SRM-II, the current rising sharply reaches its highest value at 10.5 A. It reduces to 7.6 A at the end of the dwell duration and then to zero.

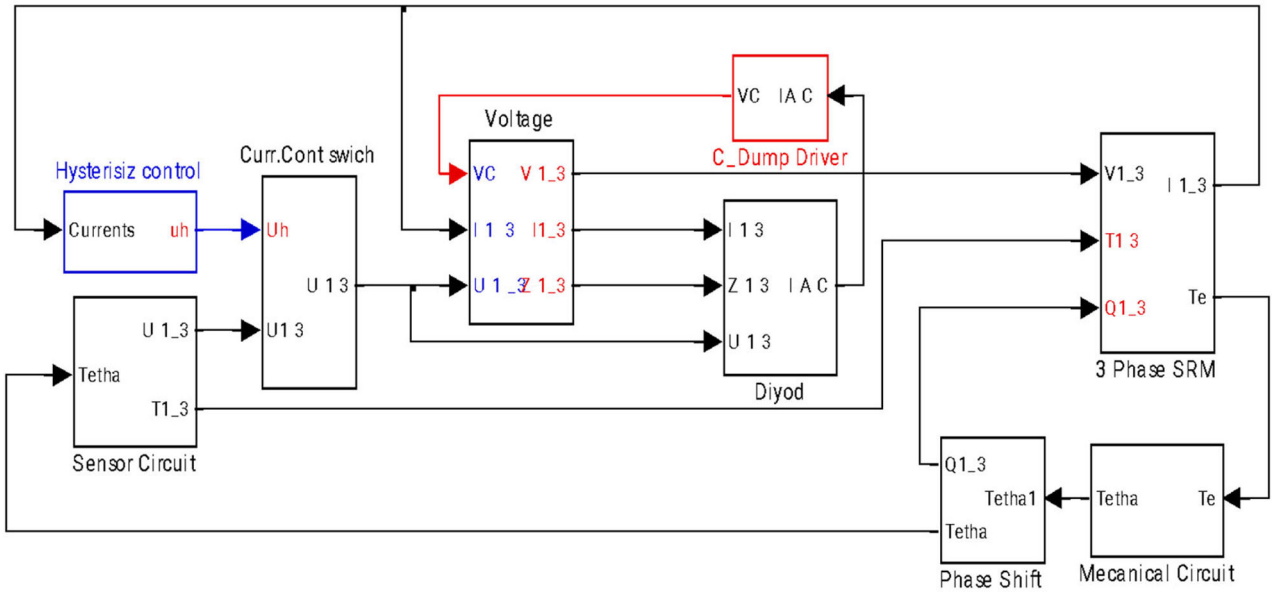

FIGURE 4. MATLAB–SIMULINK-based dynamic model of SRM.

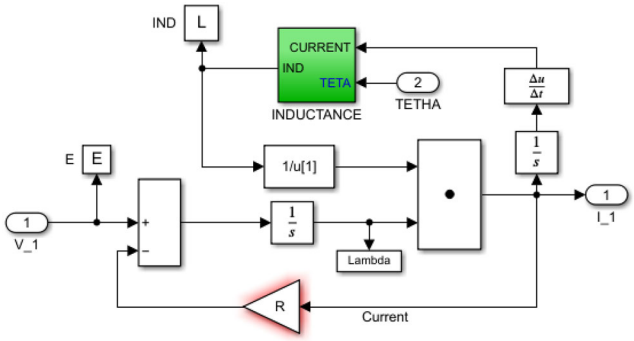

FIGURE 5. One-phase equivalent circuit of SRM.

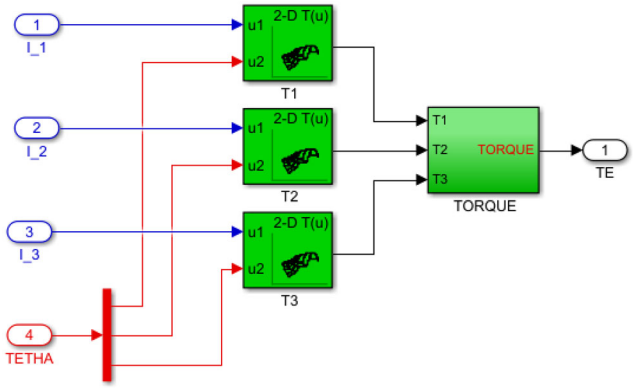

FIGURE 6. Torque circuit of SRM.

In Figure 8, 3-phase torques produced by the SRM-I and SRM-II are given as Te_1 and Te_2 respectively. Important parameters read from Figure 6 are given in detail in Table 4. Max and min torque values for SRM-I are

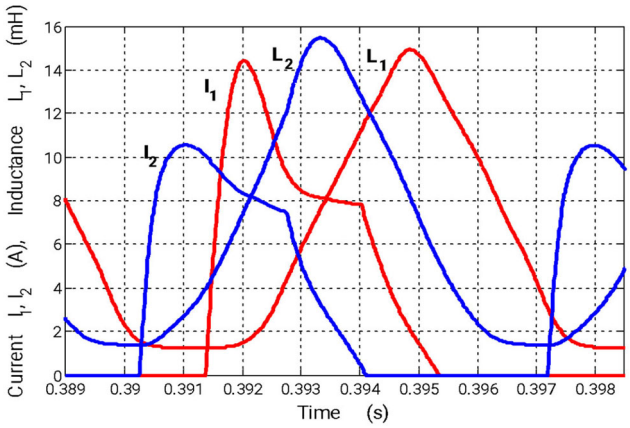

FIGURE 7. Current and inductance waveforms of SRM-I and SRM-II (UnCM).

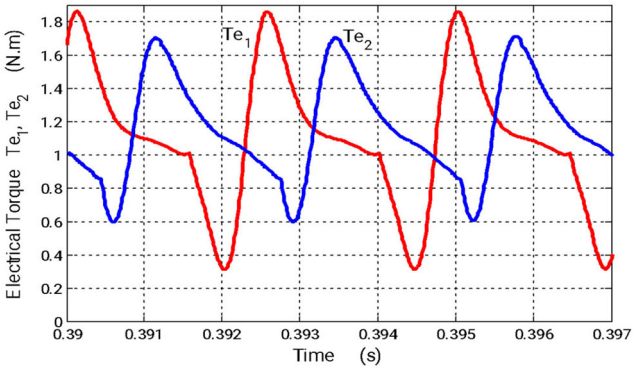

FIGURE 8. Torque waveforms of SRM-I and SRM-II (UnCM).

Symbol	SRM-I	SRM-II
T_{max}	1.86 Nm	1.70 Nm
T_{min}	0.31 Nm	0.60 Nm
T_{avg}	1.07 Nm	1.00 Nm
$\%T_r$	71.40 %	47.80 %
ΔT_r		

TABLE 4. Comparison of static and dynamic torques for SRM-I and SRM-II (UnCM).

Symbol	SRM-I	SRM-II
T_{max}	1.40 Nm	1.20 Nm
T_{min}	0.18 Nm	0.39 Nm
T_{avg}	0.79 Nm	0.79 Nm
$\%T_r$	77.20 %	62.50 %
ΔT_r	15.20%	

TABLE 5. Comparison of the electrical torques for SRM I and SRM II (CCM).

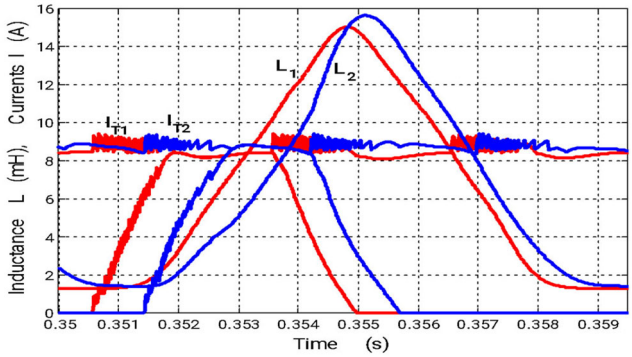

FIGURE 9. Current and inductance waveforms of SRM-I and SRM-II (CCM).

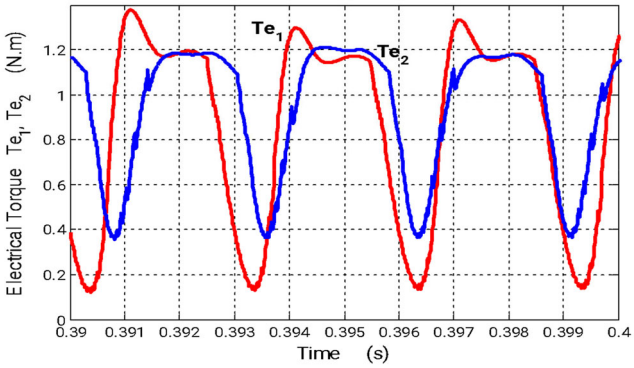

FIGURE 10. Torque waveforms of SRM-I and SRM-II (CCM).

1.86 Nm and 0.31 Nm whereas these torques are 1.7 Nm and 0.6 Nm for SRM-II respectively, as indicated in Table 4.

In Table 4, $\%T_r$ is defined as the dynamic torque ripple percentage, and DT_r is the improvement in the torque ripples. Dynamic analyses obtained in the UnCM operation give torque ripples of 71.4% and 47.8% for SRM-I and SRM-II respectively, which means an improvement of 23.6%. The fact that the static torque ripple of SRM-II is 24.1% better than that of SRM-I has been shown in a previous study [4].

Therefore, the improvements obtained from the static and dynamic analyses are almost the same (24.1% vs 23.6%); in other words, the results of both analyses subsequently support each other.

4.2. Dynamic Analysis in Time Domain for CCM

Total phase current and inductance waveforms in the time domain for the SRM-I and SRM-II are IT1, L1, and IT2, L2 in Figure 9, respectively. It can be seen that IT1 is increasing faster than IT2, as the slope of L2 inductance is less than that of L1 at the time of phase turn-on of SRM-I and SRM-II.

In this case, the total current exceeds 9 A because some amount of current flows through the other phases. While only one phase current is existing, IT2 current is also at 9 A approximately. It is noticed that IT1 rapidly drops to 8 A and almost stays constant.

Electrical torque waveforms for the SRM-I and SRM-II are shown in Figure 10. In the waveforms, T_{e1} for SRM-I reaches its maximum value at 1.4 Nm then reduces to 1.2 Nm, and afterward comes to its minimum value at 0.18 Nm. T_{e2} for SRM-II reaches its maximum value at 1.2 Nm and continues at this value during the conduction. At the end of conduction time, the torque begins to reduce and comes to a value of 0.39 Nm.

A comparison of the SRM-I and SRM-II torque values is given in Table 5. Dynamic analyses obtained in the CCM mode result torque ripples of 77.2% and 62.5% for the SRM-I and SRM-II, respectively, an improvement of 15.2%.

A 23.6% improvement is obtained in torque ripples for the UnCM and 15.2% for the CCM according to the static analyses. This difference in torque ripples of the SRM-II for UnCM operation is due to CCM operation.

4.3. Dynamic Analysis in Frequency Domain for UnCM

FFT results of the torques normalized to the fundamental frequency for SRM-I and SRM-II are shown in Figure 11

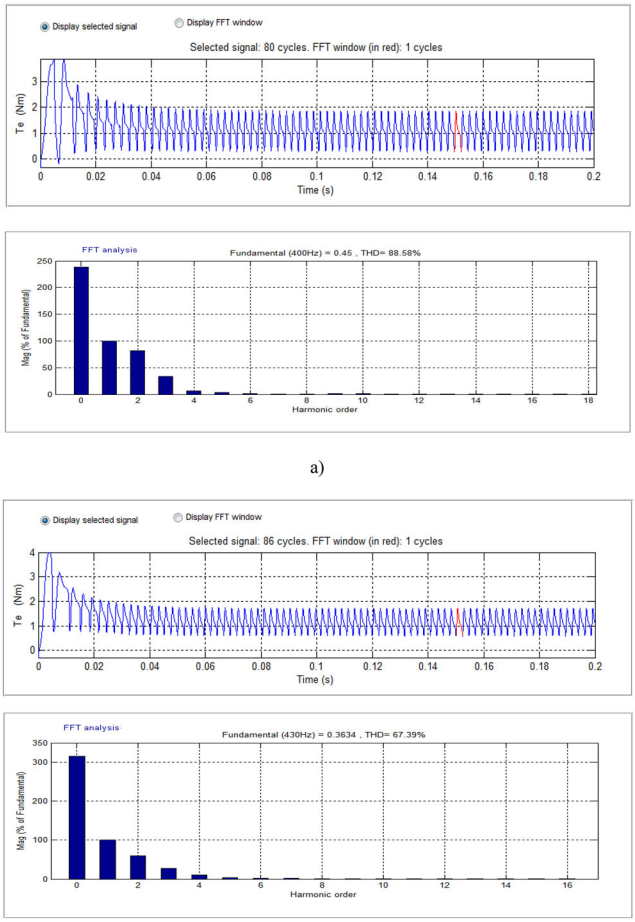

FIGURE 11. Results of FFT analysis for torque waveform (UnCM). (a) SRM-I, (b) SRM-II

in the case of the UnCM. Comparative and detailed values of the normalized torque harmonics are given in Table 6. The fundamental frequency for the SRM-I is 400 Hz. In the electrical torque waveform of SRM-I, the DC component is 1.071. 2nd, 3rd, and 4th harmonics are 81.64%, 33.34%, and 6.86% respectively. The THD value of SRM-I is 88.58%. Also, regarding the SRM-II, the fundamental frequency is 430 Hz.

DC component is 1.149. 2nd, 3rd, and 4th harmonics are 60.41%, 27.11%, and 3.95% respectively. THD values of 88.58% and 67.39% for the SRM-I and SRM-II respectively, 21.19% improvement in THD is also achieved. As can be seen from Table 6, low harmonic components that produce dominant torque ripples are reduced in the SRM-II. Although the torque ripple amplitudes in SRM-I are lower particularly at higher harmonics than that of the SRM-II, the effect of these harmonic components on torque

Sampling time = 1e–005 s		
SRM1 SRM2		
DC component = 1.071 1.149		
Fundamental = 0.3182 0.2569 (rms)		
THD	88.58%	67.39%
DC component	238.10%	316.12%
Fundamental	100.00%	100.00%
h(2)	81.64%	60.41%
h(3)	33.34%	27.11%
h(4)	6.86%	11.19%
h(5)	3.49%	3.95%
h(6)	1.82%	2.17%
h(7)	0.84%	2.17%
h(8)	0.30%	1.26%
h(9)	1.46%	1.02%
h(10)	1.23%	1.03%
h(11)	0.54%	0.70%
h(12)	0.47%	0.87%
h(13)	0.25%	0.75%
h(14)	0.36%	0.52%
h(15)	0.55%	0.55%
h(16)	0.40%	0.52%

TABLE 6. Values of FFT analysis for torque (UnCM) SRM-I and SRM-II.

ripple is not supposed to be so considerable due to inherently suppressing in the motor.

4.4. Dynamic Analysis in Frequency Domain for CCM

The normalized *FFT* torque results for SRM-I and SRM-II in the case of controlled current operation are given in Figure 12. The fundamental frequency is 340 Hz. for SRM-I and 360 Hz. for SRM-II. Comparative and detailed *FFT* of the normalized torque harmonics are given in Table 7. As shown in Table 7 for the CCM operation, the DC component is 0.846. 2nd, 3rd, and 4th harmonics are 56.40%, 11.97%, and 7.65% respectively.

The THD value of SRM-I is 58.33%. Regarding the SRM-II, the DC component is 0.96, 2nd, 3rd, and 4th harmonics are 47.43%, 13.73%, and 5.65% respectively. THD values of 58.33% and 50.02% for the SRM-I and SRM-II respectively, 8.31% improvement in THD is also achieved. Table 7 shows that low harmonic components determining the torque ripple are decreased on SRM-II.

Similarly, higher harmonic components seem to have relatively lower amplitudes in SRM-I but their influence is much less. The improvements both in torque ripple and *THD* according to the FFT analyses are given for SRM-I and SRM-II under the UnCM and the CCM operation conditions in Table 8.

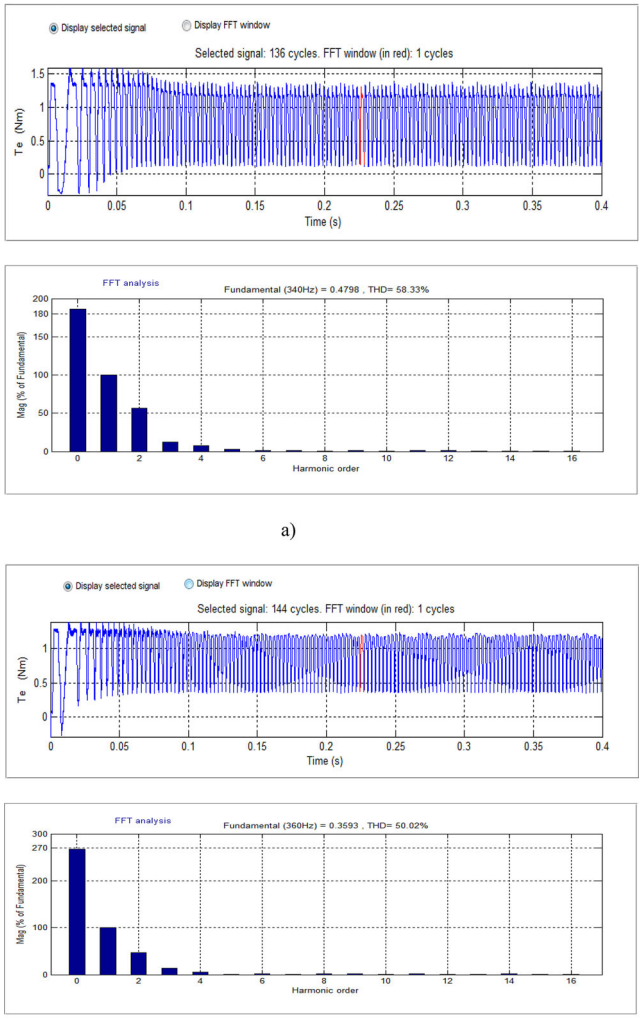

FIGURE 12. Results of FFT analysis for torque waveform (CCM). (a) SRM-I, (b) SRM-II.

5. CONCLUSION AND EVALUATION

In this study, dynamic analyses of the SRMs with a classical (SRM-I) and a new pole shape (SRM-II) with C-dump driver circuits have been performed for both the UnCM and the CCM operations and 23.6% and 15.2% torque ripple improvements in the SRM-II compared with the SRM-I have been achieved for the mentioned current operations respectively. It is concluded that the SRM-II with a modified pole shape has lower *THD* values in the *FFT* analyses than the SRM-I. When considering the SRM-I, the *THD* reductions in the SRM-II are 21.19% and 8.31% for the UnCM and the CCM operations respectively. Consequently, torque ripple due to the harmonic components on the proposed SRM-II is significantly reduced particularly for lower components.

Sampling time = 1e–005 s		
SRM1 SRM2		
DC component = 0.8946 0.96		
Fundamental = 0.3393 0.2541 (rms)		
THD	58.33%	50.02%
DC component	186.43%	267.17%
Fundamental	100.00%	100.00%
h(2)	56.49%	47.43%
h(3)	11.97%	13.43%
h(4)	7.65%	5.65%
h(5)	2.96%	1.18%
h(6)	1.35%	1.36%
h(7)	1.16%	0.45%
h(8)	0.75%	1.71%
h(9)	1.25%	1.27%
h(10)	0.45%	0.76%
h(11)	0.84%	1.76%
h(12)	1.04%	0.70%
h(13)	1.17%	1.09%
h(14)	0.72%	1.68%
h(15)	0.61%	0.82%
h(16)	0.15%	1.02%

TABLE 7. Values of FFT analysis for torque (CCM) SRM-I and SRM-II.

Type	Name	SRM-I	SRM-II
UnCM	$\%T_r$	71.4%	47.80%
	ΔT_r	23.60%	
	THD	88.58%	67.30%
	ΔTHD	21.19%	
CCM	$\%T_r$	77.20%	62.50%
	ΔT_r	15.20%	
	THD	58.33%	50.02%
	ΔTHD	8.31%	

TABLE 8. Torques under the UnCM and the CCM for SRM-I and SRM II.

REFERENCES

[1] I. Husain, "Minimization of torque ripple in SRM drives," *IEEE Trans. Indus. Electron.*, vol. 49, no. 1, pp. 28–39, Feb. 2002. DOI: 10.1109/41.982245.

[2] D. S. Schramm, B. W. Williams, and T. C. Green, "Torque ripple reduction of switched reluctance motors by phase current optimal profiling," PESC'92 Conference, 1992, pp. 857–860.

[3] J. Y. Le Chenadec, M. Geoffroy, B. Multon, and L. C. Mouchoux, "Torque ripple minimisation in switched reluctance motors by optimisation of current wave-forms and tooth shape with copper losses and "V.A. Silicon" Constraints," ICEM'94 Conf, Paris, 1994, pp. 559–564.

[4] M. Asgar, H. Torkaman, and E. Afjei, "Design, modeling and prototyping a flat switched reluctance machine for

direct-drive systems," *J. Electr. Eng. Technol.*, vol. 15, no. 1, pp. 449–456, 2020. DOI: 10.1007/s42835-018-00077-7.

[5] Y. Ozoglu, M. Garip, and E. Mese, "Torque ripple reduction in switched reluctance motors by pole tip shapings," 10th international power electronics and motion control," Epe-Pemc 2002, Cavtat & Dubrovnic, Croatia, September, pp. 9–11.

[6] M. Moallem, C. M. Ong, and L. E. Unnewehr, "Effect of rotor profiles on the torque of a switched reluctance motor," *IEEE Trans. Indus. Appl.*, vol. 28, no. 2, pp. 364–369, 1992. DOI: 10.1109/28.126743.

[7] Y. Ohdachi, Y. Kawase, Y. Miura, and Y. Hayashi, "Optimum design of switched reluctance motors using finite element analysis," *IEEE Trans. Magn.*, vol. 33, no. 2, pp. 2033–2036, 1997. DOI: 10.1109/20.582709.

[8] F. Kentli and H. Çalik, "MATLAB–SIMULINK modelling of 6/4 SRM with static data produced using finite element method," *Acta Polytech. Hung.*, vol. 8, no. 6, pp. 23–42, 2011.

[9] K. Diao, X. Sun, G. Lei, Y. Guo, and J. Zhu, "Multiobjective system level optimization method for switched reluctance motor drive systems using finite element model," *IEEE Trans. Indus. Electr.*, vol. 67, no. 12, pp. 10055–10064, 2020. DOI: 10.1109/TIE.2019.2962483.

[10] C. Changhwan, K. Seungho, Y. Kim, and K. Park, "A new torque control method of a switched reluctance motor using a torque-sharing function," *IEEE Trans. Magn.*, vol. 38, no. 5, pp. 3288–3290, 2002. DOI: 10.1109/TMAG.2002.802295.

[11] X. D. Xue, K. W. E. Cheng, and S. L. Ho, "Optimization and evaluation of torque-sharing functions for torque ripple minimization in switched reluctance motor drives," *IEEE Trans. Power Electron.*, vol. 24, no. 9, pp. 2076–2090, Sep. 2009. DOI: 10.1109/TPEL.2009.2019581.

[12] J. Ye, B. Bilgin, and A. Emadi, "An offline torque sharing function for torque ripple reduction in switched reluctance motor drives," *IEEE Trans. Energy Convers.*, vol. 30, no. 2, pp. 726–735, Jun. 2015. DOI: 10.1109/TEC.2014.2383991.

[13] D. H. Lee, J. Liang, Z. G. Lee, and J. W. Ahn, "A simple nonlinear logical torque sharing function for low-torque ripple SR drive," *IEEE Trans. Indus. Electron.*, vol. 56, no. 8, pp. 3021–3028, Aug. 2009.

[14] A. Derdiyok, N. Inanc, V. Ozbulur, and Y. Ozoglu, "Optimal phase current profiling of SRM by fuzzy logic controller to minimize torque ripple," 12th IEEE-ISIC 1997 Conf., Istanbul, Turkey, 1997, pp. 77–82.

[15] O'Donovan, J. G. Roche, P. J. Kavanagh, R. C. Egan, M. G., and J. M. D. Murphy, Neural network based torque ripple minimisation in a switched reluctance motor, IECON'94 Conf., pp. 1126–1231.

[16] C. Rochford, R. C. Kavanagh, M. G. Egan, and J. M. D. Murphy, "Development of smooth torque in switched reluctance motors using self-learning techniques," *Eur. Power Electr.*,1993, pp. 14–19.

[17] N. C. Sahoo, J. X. Xu, and S. K. Panda, "Low torque ripple control of switched reluctance motors using iterative learning," *IEEE Trans. Energy Convers.*, vol. 16, no. 4, pp. 318–326, Dec. 2001. DOI: 10.1109/60.969470.

[18] X. Sun, K. Diao, and Z. Yang, "Performance improvement of a switched reluctance machine with segmental rotors for hybrid electric vehicles," *Comput. Elect. Eng.*, vol. 77, pp. 244–259, Jul. 2019. DOI: 10.1016/j.compeleceng.2019.06.002.

[19] D.-M. Nguyen, I. Bahri, G. Krebs, E. Berthelot, and C. Marchand, "Vibration study of the intermittent control for a switched reluctance," *Math. Comput. Simulat.*, vol. 158, pp. 308–325, Apr. 2019. PagesDOI: 10.1016/j.matcom.2018.09.015.

[20] C. Gan, F. Meng, Z. Yu, R. Qu, Z. Liu, and J. Si, "Online calibration of sensorless position estimation for switched reluctance motors with parametric uncertainties," *IEEE Trans. Power Electr.*, vol. 35, no. 11, pp. 12307–12320, 2020. DOI: 10.1109/TPEL.2020.2983103.

[21] A. Rezig, W. Boudendouna, A. Djerdir, and A. N'Diaye, "Investigation of optimal control for vibration and noise reduction in-wheel switched reluctance motor used in electric vehicle," *Math. Comput. Simul.*, vol. 167, pp. 267–280, Jan. 2020. DOI: 10.1016/j.matcom.2019.05.016.

[22] H. Çalik, S. H. Undil, H. H. Çelik, and Istanbul Üniversitesi-Cerrahpaşa, Department of Electric-Electronic Engineering, 34850-Avcılar, Istanbul, Turkey, "C-dump converter design and its dynamic analysis in Simulink environment for a switch reluctance machine," *IJEAT*, vol. 9, no. 1, pp. 5144–5148, Oct. 2019. DOI: 10.35940/ijeat.A1753.109119.

BIOGRAPHIES

Hüseyin Çalik was born in Giresun, Turkey in 1967. He received the B.Sc, M.Sc.and degrees in Electrical Engineer from Marmara University, Turkey, in 1999 and 2005. He worked as a Ass. Professor and head of Electric Programme in Vocational School of Technology in Istanbul University cerrahpaşa. He is currently professor, Giresun University, Department of Electrical-Electronics Engineering, Giresun/Turkey. His research interests are in the areas of industrial automation systems, computer aided design, control of electrical machines, adjustable-speed drives, fuzzy logic and neural network applications.

Yusuf Özoğlu was born in Urgup, Turkey in 1967. He received the B.S., M.S., and Ph.D. degrees in electrical engineering and M.S. degrees in electrical engineering from Istanbul Technical University, Istanbul, Turkey, in 1989, 1995 and 1999, respectively. He has been working as a professor since 2018 at Istanbul University-Cerrahpasa, where he started working as an research assistant in 1991. His research interests are electrical machine design and optimizations of design parameters, especially using the finite element method.

S. Hakan Undil was born in Istanbul, Turkey, 1959. He received both B.Sc. and M.Sc. degrees in Electronics and Telecommunication Engineering from Faculty of Electrical and Electronics Engineering in Istanbul Technical University. He

received his Ph.D. degree in Electrical Engineering from the Institute of Science and Technology in Yıldız Technical University in 1994. He worked as a professor and head of Electronics Technology Programme in Vocational School of Technology in Istanbul University. He is currently professor at Electrical and Electronics Department of Engineering and Architect Faculty at Nisantasi University. His research interests include modeling and simulation, power electronics, control of electrical machines.

Ümit Kemallettin Terzi was born in Zonguldak in 1968. He received his B.S. degree from Electrical Education Department of Technical Education Faculty of University of Marmara, Istanbul, in 1989 and his M.Sc. and Ph.D. degree from Electrical Education Department of Institute of Pure and Applied Sciences, University of Marmara, Istanbul, in 1994 and 2000 respectively. From 1989 to 1996, he worked as a research assistant, from 1996 to 2000 as a lecturer, from 2000 to 2013 as an Assistant Prof. Dr. for University of Marmara. Since 2013 he has been working as an Associate Prof. Dr. for Electrical and Electronics department of Technology Faculty of Marmara University and Electrical Education Department of Technical Education Faculty where he is head of department. His research interests include electric power components and systems.